Antigen-loaded Dendritic Cell Migration: MR Imaging in a Pancreatic Carcinoma Model[1]

Zhuoli Zhang, MD, PhD
Weiguo Li, PhD
Daniele Procissi, PhD
Kangan Li, MD, PhD
Alexander Y. Sheu, MD
Andrew C. Gordon, MS
Yang Guo, MD
Khashayarsha Khazaie, PhD
Yi Huan, MD, PhD
Guohong Han, MD, PhD
Andrew C. Larson, PhD

Purpose: To test the following hypotheses in a murine model of pancreatic cancer: *(a)* Vaccination with antigen-loaded iron-labeled dendritic cells reduces T2-weighted signal intensity at magnetic resonance (MR) imaging within peripheral draining lymph nodes (LNs) and *(b)* such signal intensity reductions are associated with tumor size changes after dendritic cell vaccination.

Materials and Methods: The institutional animal care and use committee approved this study. Panc02 cells were implanted into the flanks of 27 C57BL/6 mice bilaterally. After tumors reached 10 mm, cell viability was evaluated, and iron-labeled dendritic cell vaccines were injected into the left hind footpad. The mice were randomly separated into the following three groups (n = 9 in each): Group 1 was injected with 1 million iron-labeled dendritic cells; group 2, with 2 million cells; and control mice, with 200 mL of phosphate-buffered saline. T1- and T2-weighted MR imaging of labeled dendritic cell migration to draining LNs was performed before cell injection and 6 and 24 hours after injection. The signal-to-noise ratio (SNR) of the draining LNs was measured. One-way analysis of variance (ANOVA) was used to compare Prussian blue–positive dendritic cell measurements in LNs. Repeated-measures ANOVA was used to compare in vivo T2-weighted SNR LN measurements between groups over the observation time points.

Results: Trypan blue assays showed no significant difference in mean viability indexes (unlabeled vs labeled dendritic cells, 4.32% ± 0.69 [standard deviation] vs 4.83% ± 0.76; P = .385). Thirty-five days after injection, the mean left and right flank tumor sizes, respectively, were 112.7 mm^2 ± 16.4 and 109 mm^2 ± 24.3 for the 1-million dendritic cell group, 92.2 mm^2 ± 9.9 and 90.4 mm^2 ± 12.8 for the 2-million dendritic cell group, and 193.7 mm^2 ± 20.9 and 189.4 mm^2 ± 17.8 for the control group (P = .0001 for control group vs 1-million cell group; P = .00007 for control group vs 2-million cell group). There was a correlation between postinjection T2-weighted SNR decreases in the left popliteal LN 24 hours after injection and size changes at follow-up for tumors in both flanks (R = 0.81 and R = 0.76 for left and right tumors, respectively).

Conclusion: MR imaging approaches can be used for quantitative measurement of accumulated iron-labeled dendritic cell–based vaccines in draining LNs. The amount of dendritic cell–based vaccine in draining LNs correlates well with observed protective effects.

Online supplemental material is available for this article.

[1] From the Department of Radiology (Z.Z., W.L., D.P., K.L., A.Y.S., A.C.G., Y.G., A.C.L.), Robert H. Lurie Comprehensive Cancer Center (Z.Z., K.K., A.C.L.), and Department of Biomedical Engineering (A.C.L.), Northwestern University, 737 N Michigan Ave, 16th Floor, Chicago, IL 60611; Department of Radiology, Xijing Hospital, Fourth Military Medical University, Xi'an, China (Z.Z., Y.H., A.C.L.); and Department of Digestive Diseases, Xijing Hospital, Fourth Military Medical University, Xi'an, China (G.H.). Received September 15, 2013; revision requested November 19; revision received April 9, 2014; accepted July 9; final version accepted July 14. Supported by the American Cancer Society (grant SP0011492) and the National Natural Science Foundation of China (grant NSFC81220108011). **Address correspondence to** Z.Z. (e-mail: *zhuoli-zhang@northwestern.edu*).

Dendritic cells are one of the most potent antigen-presenting cells in the immune system, particularly because of their ability to directly prime naive T cells in lymph nodes (LNs) (1,2). Dendritic cells are important in the initiation and regulation of antigen-specific immune responses and have been used as potent therapeutic vaccines against human cancers (2,3). They are highly malleable antigen-presenting cells that can promote potent antitumor immunity and tolerance, depending on the environmental signals received. Dendritic cell–based vaccination strategies offer the potential for systemic treatment of many cancers (4–6).

Results of recent studies (7–9) have shown that when vitro techniques utilize dendritic cells pulsed with exogenous tumor antigens, the antigen-loaded dendritic cells are then adoptively transferred to the hosts as cancer vaccines to enhance immune response. These in vitro loading approaches permit better control of the environment in which dendritic cells interact with antigens while avoiding potential pitfalls associated with in vivo immunization procedures (7). However, clinical trials (7,10–12) have not yet demonstrated positive therapeutic efficacy or a clear indication for dendritic cell vaccines. Given that the effectiveness of immunization with antigen-loaded dendritic cells is strongly influenced by their successful migration to peripheral draining LNs, in vivo measurements of dendritic cell migration activity could serve as an early biomarker for prediction of therapy response in individual patients, prompting additional vaccinations or adoption of alternative therapeutic strategies when necessary.

In animal models, dendritic cell migration and subsequent interactions within T-lymphocytes in the LNs can be studied by using fluorescence imaging techniques (13,14). Investigators (15,16) have sought to translate these dendritic cell tracking approaches into clinical settings by using nuclear imaging and magnetic resonance (MR) imaging methods. Nuclear imaging methods can be highly sensitive for dendritic cell detection but offer relatively poor spatial resolution. Study results (16–19) have demonstrated the potential of using superparamagnetic iron oxide (SPIO) labeling techniques for in vivo MR imaging visualization of dendritic cell migration to LNs in animal models and in patients with melanoma. Additional studies are necessary to compare these MR imaging measurements of dendritic cell migration with longitudinal tumor response after vaccination.

The purpose of our study was to test the following hypotheses in a murine model of pancreatic ductal cell adenocarcinoma: *(a)* Vaccination with antigen-loaded SPIO-labeled dendritic cells reduces T2-weighted signal intensity within peripheral draining LNs and *(b)* resulting longitudinal tumor size changes after dendritic cell vaccination are associated with the magnitude of these T2-weighted signal intensity reductions.

Advances in Knowledge

- With use of iron nanoparticles in combination with protamine sulfate cell-labeling techniques, the 3-hour labeling time in our study resulted in 100% labeling efficiency and no decrease in cellular viability.
- There was a strong negative correlation between T2-weighted signal-to-noise ratio decreases in the left popliteal lymph node 24 hours after injection and tumor size changes at follow-up (R = 0.81 and R = 0.76 for left and right tumors, respectively).

Materials and Methods

This study was approved by the institutional animal care and use committee of Northwestern University.

Pancreatic Ductal Adenocarcinoma Cell Line and Mouse Model

The mouse Panc02 cell line is derived from amethylcholanthrene-induced pancreatic ductal adenocarcinoma in C57BL/6 mice and was purchased from the American Type Culture Collection (Rockville, Md). Panc02 cells were maintained in RPMI 1640 medium (Life Technologies, Carlsbad, Calif) supplemented with glutamine (2 mmol/L, Life Technologies), pyruvate (1 mmol/L, Sigma-Aldrich, St Louis, Mo), penicillin and streptomycin (100 IU/mL, Sigma-Aldrich), and 10% fetal bovine serum (Sigma-Aldrich). The cells were maintained in a humidified atmosphere of 5% CO_2 at 37°C. Before implantation, cell viability was assessed by means of trypan blue (Sigma-Aldrich) staining (cell viability of > 90% was confirmed prior to tumor implantation). Twenty-seven female C57BL/6 mice (4 weeks of age, weighing between 13 and 17 g; Charles River, Wilmington, Mass) were used for our study. Early passage Panc02 cells were harvested, and approximately 1×10^6 cells suspended in 200 μL of phosphate-buffered saline were subcutaneously implanted into the left and right flanks of each mouse.

Generation and Antigen Loading of Bone Marrow–derived Dendritic Cells

Bone marrow–derived dendritic cells were prepared as previously described (20). Briefly, bone marrow cells were

Published online before print
10.1148/radiol.14132172 **Content codes:** GI MI

Radiology 2015; 274:192–200

Abbreviations:
ANOVA = analysis of variance
LN = lymph node
ROI = region of interest
SNR = signal-to-noise ratio
SPIO = superparamagnetic iron oxide

Author contributions:
Guarantors of integrity of entire study, Z.Z., G.H.; study concepts/study design or data acquisition or data analysis/interpretation, all authors; manuscript drafting or manuscript revision for important intellectual content, all authors; manuscript final version approval, all authors; literature research, Z.Z., W.L., A.C.G., K.K., G.H.; experimental studies, all authors; statistical analysis, Z.Z., W.L., K.L., G.H.; and manuscript editing, Z.Z., D.P., A.C.G., Y.G., K.K., Y.H., G.H., A.C.L.

Funding:
This research was supported by the National Institutes of Health (grants NCI CA134719 and UL1RR0254741).

Conflicts of interest are listed at the end of this article.

See also Science to Practice in this issue.

isolated from femur and tibia. After red blood cell lysis, cells were cultured in dendritic cell medium. After 7 days, loosely adherent cells were harvested. Next, dendritic cells were stained with the following antibodies: APC antimouse CD86 (BD Pharmingen, San Jose, Calif) and PE antimouse CD40 (BD Pharmingen). Finally, fluorescence-activated cell sorter analysis was performed with a flow cytometer, and the results were analyzed with FlowJo Software (Tree Star, Ashland, Ore) (sample size, $n = 6$). The expression of dendritic cell markers was quantified as positive and negative percentages. For antigen loading of dendritic cells, generated dendritic cells were co-cultured with apoptotic Panc02 cells, as previously described (21,22). A more detailed description of the generation and antigen loading of these dendritic cells is included in Appendix E1 (online).

Iron Oxide Nanoparticle Labeling of Antigen-loaded Dendritic Cells

Antigen-loaded dendritic cells were placed in a flask with fresh dendritic cell medium and protamine sulfate–coated (Sigma-Aldrich) Texas Red SPIO nanoparticles (GENOVIS, Lund, Sweden), and final concentrations of 20 μg iron per milliliter and 0.5 μg protamine sulfate per milliliter were used for labeling the antigen-loaded dendritic cells. The dendritic cells were then incubated for 3 hours at 37°C in a 5% CO_2 atmosphere to permit cellular uptake of the SPIO particles. Aliquots of labeled cells and unlabeled (control) cells were stained with trypan blue. Dead (trypan blue–positive) and live cells were counted to calculate overall viability (expressed as a percentage of overall cells counted). Labeling efficiency was determined by using fluorescence microscopy. Additional procedural details are included in Appendix E1 (online).

The average amount of iron taken up per cell was measured by using nuclear MR relaxometry measurements, as previously described (23). Digestion of approximately 2×10^5 labeled cells in 1 mL of 6M HCl was performed for 1 hour at room temperature, and the cells were then placed into individual wells in 96-well solid plate (glass). Eight standard samples with iron concentrations ranging from 0 to 10 μg/mL were prepared by diluting 1000-ppm iron atomic absorption standard solution (Sigma-Aldrich); these samples were pipetted into adjacent wells of the plate. The plate containing digested cells and iron standard solution was placed into a 7.0-T high-field-strength small-animal MR imaging system (ClinScan; Bruker Biospin, Ettlingen, Germany), and T2-weighted images were obtained with the following parameters: a Carr-Purcell-Meiboom-Gill sequence with four echoes per excitation; repetition time msec/echo times msec, 2000/14.1, 28.2, 42.3, 56.4; field of view, 50×50 mm^2; matrix, 256×256; and section thickness, 2 mm. An offline voxelwise postprocessing algorithm was implemented in the Matlab software package, version 7.1 (MathWorks, Natick, Mass) and was used to generate T2 maps (assuming monoexponential voxelwise echo time–dependent signal decay in respective Carr-Purcell-Meiboom-Gill images). T2 values for circular regions of interest (ROIs) (5 mm) were defined within each well. A standard curve was constructed by plotting R2 = 1/T2 versus [Fe] for the iron standards. The iron concentration in each digested cell sample was then calculated from its R2 value by means of linear interpolation of this standard curve. Finally, iron concentrations were normalized by the actual number of cells digested in each sample to give the average iron content in picograms of iron per cell and were averaged over the digestion of six separately cultured cell populations labeled in identical conditions ($n = 6$).

Therapeutic Vaccination Strategy

A study flowchart is included in Figure E1 (online). Each mouse was treated separately when one or both tumors had reached approximately 10 mm in greatest diameter. SPIO-labeled dendritic cells, in a final volume of 200 mL phosphate-buffered saline, were injected subcutaneously into the left hind footpad. Mice in group 1 ($n = 9$) were injected with 1 million labeled dendritic cells, mice in group 2 ($n = 9$) were injected with 2 million labeled dendritic cells, and control mice ($n = 9$) were injected with 200 mL phosphate-buffered saline.

In Vivo MR Imaging of Labeled Dendritic Cell Migration to LNs

MR imaging studies were performed by using a 7.0-T high-field-strength small-animal MR imaging system with a commercial mouse coil (ClinScan; Bruker Biospin) before dendritic cell injection and at 6 and 24 hours after injection. Body temperature was monitored continuously and was controlled with a water bed (SA Instruments, Stony Brook, NY). T2-weighted localization images were acquired in both the coronal and axial planes. High-spatial-resolution T1- and T2-weighted images of the popliteal LNs on each side were acquired in both the coronal and axial planes. Of note, the left popliteal LN is the first LN station that dendritic cells can migrate to after injection into the left footpad; thus, the popliteal LN was chosen for serial follow-up monitoring with MR imaging (24). The parameters for in vivo measurements were as follows for the T2-weighted turbo spin-echo sequence: 3000/44; field of view, 35×35 mm^2; matrix, 256×256; turbo factor, 12; section thickness, 0.14 mm; isotropic in-plane resolution, 0.14 mm; with acquisition synchronized to the respiratory cycle to minimize motion artifacts. The parameters for the T1-weighted segmented turbo-flash gradient-echo sequence with an inversion-recovery preparatory pulse were as follows: 1300/2.15; field of view, 35×35 mm^2; matrix, 256×256; section thickness, 0.14 mm; and isotropic in-plane resolution, 0.14 mm. Both the T1-weighted and the T2-weighted MR images were acquired with and without fat suppression.

Ex Vivo Assessment of Labeled Dendritic Cells in the Popliteal LN

The popliteal LNs on each side were harvested for histologic analysis ($n = 3$ in each group) 24 hours after dendritic cell injection. LNs were snap frozen in Optimal Cutting Temperature compound and were sliced at 4-μm

intervals. For Prussian blue staining (Sigma-Aldrich), these slices were rinsed in distilled water, incubated in a 1:1 solution of 10% aqueous solution of potassium ferrocyanide and 20% hydrochloric acid for 30 minutes, and then rinsed and counterstained with Nuclear Fast Red. For immunohistochemistry staining, tissue slices from the popliteal LN (from both sides, $n = 6$ in each group) were stained with dendritic cell marker mouse anti-CD11c and macrophage marker anti-F4/80 antibodies (Abcam, Cambridge, Mass) as previously described (25,26).

Antitumor Efficacy of Dendritic Cell Vaccination

After dendritic cell injection, vital signs; mental status, including abnormal behavior or activity; diet; and activity levels for each animal were observed daily. Tumor growth was assessed as the product of perpendicular diameters measured with a caliper; tumor size was calculated by using the tumor size formula longest length × longest width ($n = 6$ mice with 12 tumors in each group) (27). The tumor sizes were measured at multiple time points after the administration of dendritic cells (1, 5, 10, 15, 20, 25, 30, and 35 days after tumor cell implantation). All mice were euthanized 35 days after dendritic cell or control injection.

Image Analysis

For MR imaging examinations, image analyses were performed by using ImageJ (version 1.34s; National Institutes of Health, Bethesda, Md). ROIs were drawn by a radiologist (Z.Z.) with more than 15 years of experience. A circular ROI (mean diameter, 2.51 mm ± 0.32 [standard deviation]) encompassing each respective LN was used to measure mean T2-weighted signal intensity (SI_{mean}) Separate ROIs were drawn over ipsilateral caudal thigh muscles and outside the LN (drawn at consistent positions between repeated measurements with consistent sizes) to estimate relative noise levels on the basis of the standard deviation of the background signal (N_{SD}). These calculations were used to estimate the relative signal-to-noise ratio (SNR) = SI_{mean}/N_{SD} for each measurement. Prussian blue–stained slides from LN specimens (six slices from each left and right popliteal LN) were scanned at a magnification of ×20 and digitized by using the TissueFAXS system (TissueGnostics, Los Angeles, Calif). These acquired images were analyzed by using the HistoQuest Cell Analysis Software package (TissueGnostics) to quantify the total number of SPIO-labeled dendritic cells within each specimen (SPIO-labeled dendritic cells were identified on the basis of positive blue staining).

The anti-CD11c and anti-F4/80 antibody–stained slides (six from each left and right popliteal LN) were scanned, and images were digitized by using the TissueFAXS system. The images were analyzed by using the HistoQuest Cell Analysis Software to quantify the total number of CD11c-positive dendritic cells and F4/80-positive macrophages.

Statistical Analysis

Statistical calculations were performed by using the Prism V6 software package (Graphpad, La Jolla, Calif). $P < .05$ was considered to indicate a significant difference. Repeated-measures analysis of variance (ANOVA) (28) was used to compare in vivo T2-weighted SNR LN measurements between groups (1 or 2 million cells) over the observation time points (before injection and 6 and 24 hours after injection). The interactions between treatment group and time on SNR changes were analyzed. Pairwise comparisons were performed if the treatment-time interaction was significant. One-way ANOVA was used to compare Prussian blue–positive dendritic cell, CD11c-positive dendritic cell, and F4/80-positive macrophage measurements in LN. Finally, for therapeutic efficacy studies at each postinjection observation interval, the Dunnett test was used to compare left flank tumor size measurements in control and treated animals. Significant multiplicity-adjusted P values and 95% confidence intervals were reported. Pearson correlation coefficients were calculated to assess the relationship between 24-hour postinjection LN SNR changes and corresponding tumor size changes at 35 days after injection. The latter comparisons were separately performed for right and left flank tumors.

Figure 1

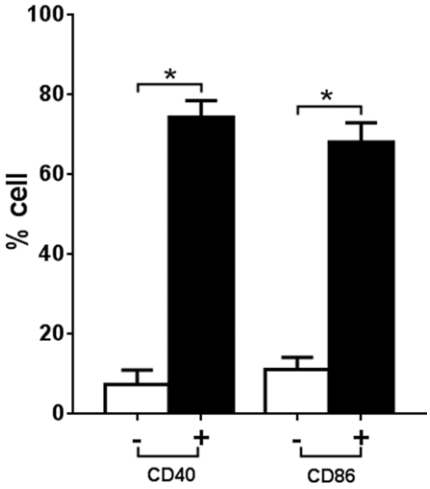

Figure 1: Bar graph shows results of flow cytometry analysis of CD40 and CD86 expression in bone marrow–derived dendritic cells. The percentages of dendritic cells positive for CD40 and those positive for CD86 were 74.4% ± 4.1 and 69.2% ± 4.8, respectively. * = $P < .05$.

Results

The mean percentages of dendritic cells positive for CD40 and CD86 were 74.4% ± 4.1 and 69.2% ± 4.8, respectively ($n = 6$) (Fig 1). Nuclear MR relaxometry measurements of iron concentrations in an acid digestion of iron-labeled dendritic cells indicated an average uptake of 0.65 pg iron per cell ± 0.03 (range, 0.48–0.73 pg iron per cell) ($n = 6$). Fluorescence microscopy of iron-labeled dendritic cell vaccines revealed extensive but nonuniform uptake of Texas Red nanoparticles in the cytoplasm (Fig 2). Labeling efficiency was 100%: All dendritic cells were labeled with SPIO ($n = 6$). There were no significant differences in viability indexes between labeled and unlabeled dendritic cells (4.32% ± 0.69 [range, 3.53%–5.32%] vs 4.83% ± 0.76 [range, 3.41%–5.62%], respectively; $P = .385$) (Fig 2, *D*).

The left popliteal LN demonstrated a marked decrease in T2-weighted

Figure 2

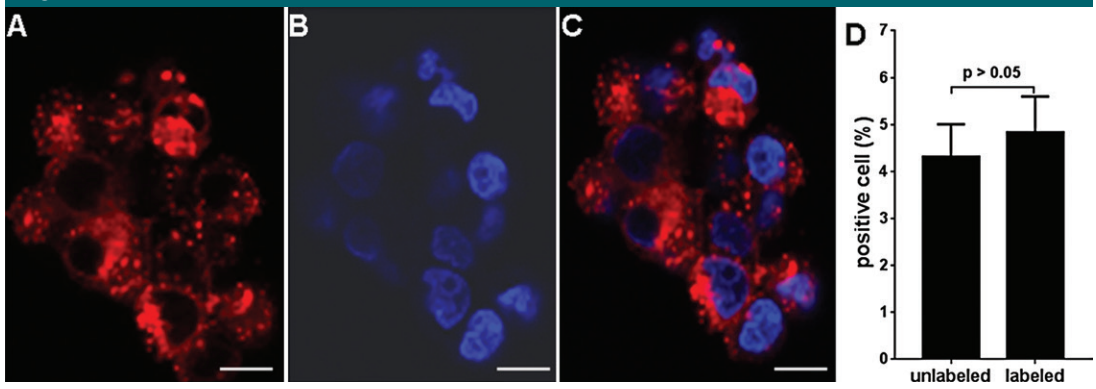

Figure 2: *A–C,* Images from fluorescence microscopy of iron-labeled dendritic cell vaccines and, *D,* results of trypan blue assessment of labeled dendritic cells. *A,* Texas Red particle accumulation is observed in cytoplasm while, *B,* DAPI-stained nuclei were blue, with coregistration in, *C,* a merged image. *D,* Bar graph shows that there was no significant difference between trypan blue viability indexes for labeled and those for unlabeled dendritic cells. Scale bars for *A, B,* and *C* = 10 μm.

Figure 3

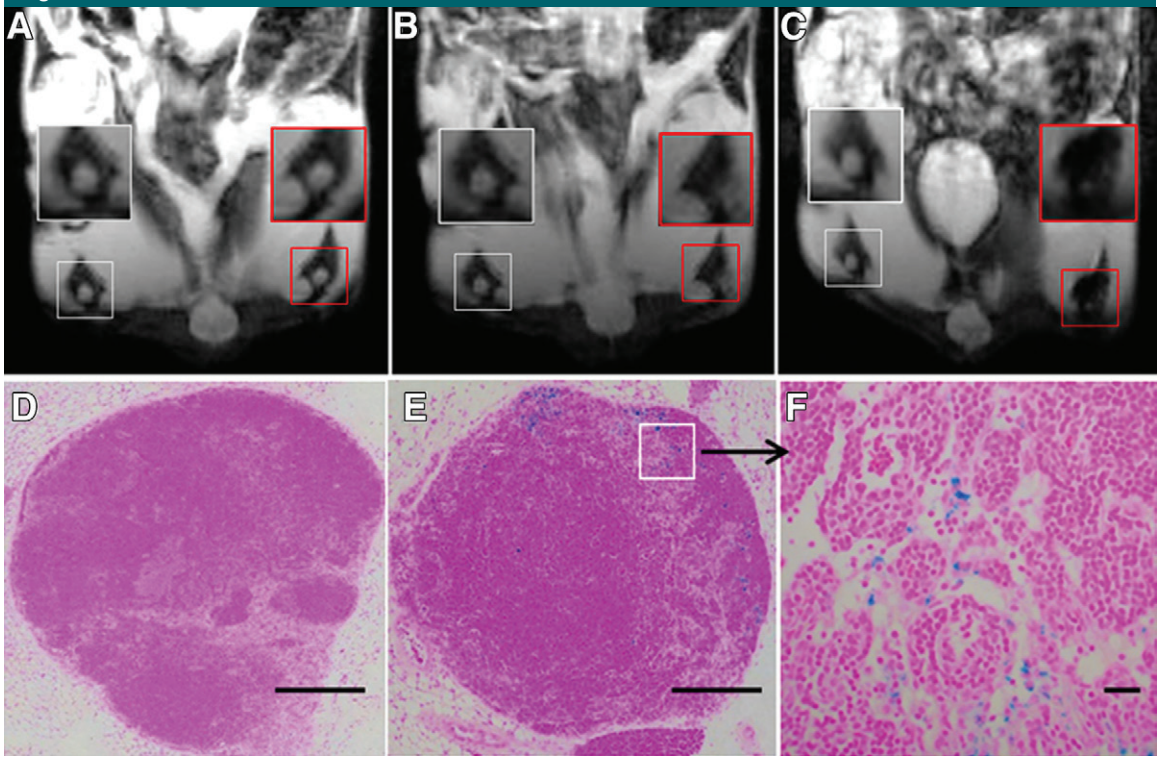

Figure 3: *A–C,* Representative coronal T2-weighted MR images of bilateral popliteal LNs in a mouse model of pancreatic carcinoma after injection of 1 million labeled dendritic cells into the left footpad. Images were obtained, *A,* prior to dendritic cell administration, *B,* 6 hours after injection, and, *C,* 24 hours after injection. White boxes = right popliteal LNs, red boxes = left popliteal LNs. *D, E,* Corresponding Prussian blue–stained slices from popliteal LNs (collected immediately after 24-hour postinjection MR imaging) in, *D,* right popliteal LN, and, *E,* left popliteal LN. *F,* High-magnification image corresponding to the inset (square) in *E.* Scale bars for *D* and *E* = 5 mm; scale bar for *F* = 50 μm.

signal intensity at both 6- and 24-hour intervals after injection, while there was no signal intensity change in the right popliteal LN at the same time points (Fig 3). Prussian blue staining of bilateral popliteal LNs (collected immediately after 24-hour postinjection MR imaging was performed) confirmed the presence of SPIO-labeled dendritic

Figure 4

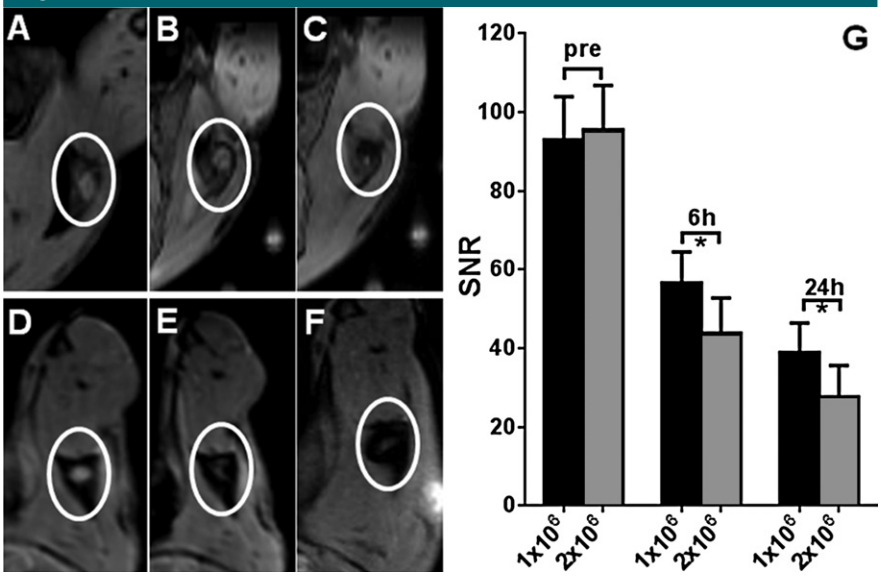

Figure 4: *A–F,* Representative T2-weighted MR images of left popliteal LN in different dendritic cell injection groups at different time points. *A–C,* Images in mouse in 1-million dendritic cell injection group, *A,* before dendritic cell injection, *B,* 6 hours after injection, and, *C,* 24 hours after injection. *D–F,* Images in mouse in 2-million dendritic cell injection group, *D,* before dendritic cell injection, *E,* 6 hours after injection, and, *F,* 24 hours after injection. *G,* Bar graph shows T2-weighted SNR measurements in the left popliteal LN 6 and 24 hours after injection compared with preinjection SNR levels in both the 1-million and 2-million dendritic cell injection groups. $* = P < .05$.

Figure 5

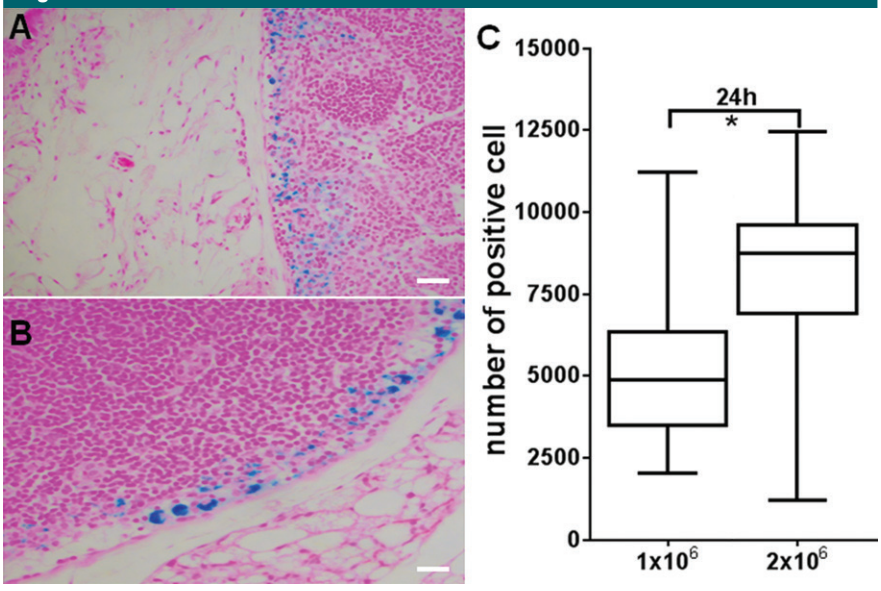

Figure 5: *A, B,* Representative Prussian blue–stained slices from left popliteal LNs 24 hours after injection for, *A,* mice in the 1-million dendritic cell injection group, and, *B,* mice in the 2-million dendritic cell injection group. *C,* Bar graph shows that there was significantly greater positive staining in the 2-million dendritic cell injection group than in the 1-million dendritic cell injection group. $* = P < .05$. Scale bars = 50 μm.

cells in left popliteal LNs, which was not observed in right popliteal LNs (Fig 3, *D* and *F*). Representative axial T2-weighted images from animals in groups 1 and 2 are shown in Figure 4. For repeated-measures ANOVA, there was a significant interaction between time (P = .00006), treatment (P = .0425), and time treatment (P = .0072) for T2-weighted SNR within the left popliteal LN. For each treatment, SNR levels decreased significantly over time in both group 1 and group 2 (Fig 4, *G*) (for the 1-million dendritic cell injection group, the preinjection SNR was 93.01 ± 10.90, while the 6-hour postinjection SNR was 56.67 ± 7.85 [P = .00009] and the 24-hour postinjection SNR was 38.93 ± 7.52 [P = .0001]; for the 2-million dendritic cell injection group, the preinjection SNR was 95.59 ± 11.28, while the 6-hour postinjection SNR was 43.86 ± 8.95 [P = .00007] and the 24-hour postinjection SNR was 27.7 ± 7.91 [P = .0001]). Moreover, there were significant differences between groups 1 and 2 at each postinfusion time point (P = .005 at 6 hours and P = .001 at 24 hours) (Fig 4, *G*). There was a significantly larger number of positively stained dendritic cells measured in the 2-million dendritic cell injection group than in the 1-million dendritic cell injection group (P = .004) (Fig 5). The quantitative results of CD11c-positive dendritic cell and F4/80-positive macrophage measurements are shown in Figure E2 (online).

The immunotherapeutic efficacy of the dendritic cell vaccination procedure was evident as inhibition of tumor growth compared with that in untreated control animals 20–35 days after vaccination (Fig 6). However, Dunnett multiple comparison tests did not demonstrate significant multiplicity-adjusted P values for comparisons of mean tumor sizes relative to control left flank tumors (P = .18–.40). There were no significant differences in therapeutic response elicited in left tumors and right tumors for each vaccination group at any time point (P = .19–0.60) (Fig 6, *A*). There were differences between tumor sizes for mice in the 1-million and 2-million dendritic cell injection groups

Figure 6

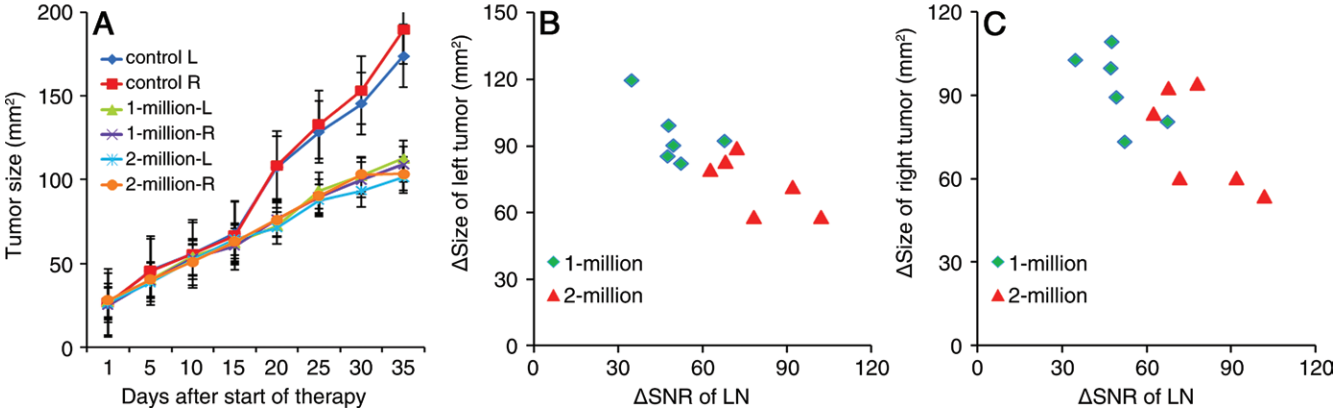

Figure 6: *A,* Graph shows tumor growth curves. Effective inhibition of tumor growth can be observed 20 days after dendritic cell vaccination ($P < .0001$ for all); no significant difference in therapeutic response was observed between tumors in the left *(L)* and right *(R)* flanks for the vaccinated groups at any time point. Significant differences were observed between the 1-million and 2-million dendritic cell injection groups 30 days after dendritic cell vaccination ($P < .0001$). *B, C,* Graphs show comparisons between T2-weighted MR imaging measurements (SNR changes in the left popliteal LN 24 hours after injection) and longitudinal therapeutic response (tumor size changes) for, *B,* left flank tumors and, *C,* right flank tumors ($R = 0.81$ and $R = 0.76$, respectively).

30–35 days after vaccination (Fig 6, *A*), but these were not significant at multiple-comparison testing ($P = .12$). Thirty-five days after injection, the relative sizes of the left and right flank tumors, respectively, were 112.7 $mm^2 \pm 16.4$ and 109 $mm^2 \pm 24.3$ for mice in the 1-million dendritic cell injection group, 92.2 $mm^2 \pm 9.9$ and 90.4 $mm^2 \pm 12.8$ for mice in the 2-million dendritic cell injection group, and 193.7 $mm^2 \pm 20.9$ and 189.4 $mm^2 \pm 17.8$ for mice in the control group ($P = .0001$ for 1 million vs 2 million; $P = .0001$ for control vs 1 million; $P = .00007$ for control vs 2 million). There was a strong negative correlation between 24-hour postinjection T2-weighted SNR decreases in the left popliteal LN and size change at follow-up for tumors in both the left and right flanks ($R = 0.81$ and $R = 0.76$ for left and right tumors, respectively) (Fig 6).

Discussion

The immunizing ability of antigen-loaded dendritic cells is strongly influenced by their migration to peripheral draining LNs. Serial monitoring of dendritic cell migration after vaccination may be critical to elucidate the potential causes of the differential response rates in patients with cancer during clinical trials. In vivo migration measurements may also be useful for early prediction of therapy response to prompt additional vaccinations or adoption of alternative therapeutic strategies when needed. Our study describes a vaccination protocol wherein dendritic cells were loaded with both tumor antigens and SPIO nanoparticles for in vivo MR imaging monitoring of SPIO-labeled dendritic cell migration shortly after therapeutic vaccination. During our study in a murine model of pancreatic carcinoma, we showed that MR imaging measurements permitted in vivo monitoring of SPIO-labeled dendritic cell–based vaccine migration to the draining LNs, which led to a reduction in the draining LN signal intensity on T2-weighted MR images. Histologic measurements confirmed that these signal intensity reductions were due to SPIO-labeled dendritic cell migration to the left popliteal LN. These signal intensity reductions, measured within 24 hours of vaccination, were well correlated with longitudinal therapeutic responses (tumor growth inhibition 35 days after vaccination).

Murine myeloid dendritic cells have been widely used to evaluate the efficacy of dendritic cell–based vaccines (29,30). These dendritic cells can be pulsed with tumor lysates (18–20), tumor protein extracts (31–33), or synthetic peptide tumor epitopes (34) or can be fused with irradiated tumor cells (35) to generate protective immunity to subsequent tumor challenges. Previous studies in the Panc02 tumor model have shown that dendritic cells pulsed with tumor lysates can readily prime tumor-specific cytotoxic T-lymphocytes (36), which motivated our selection of a similar protocol for our study. We used Panc02 tumor lysates as the antigen source, with a pulsing strategy similar to that of protocols previously approved for clinical trials of dendritic cell vaccination (21,22,27,36–38). Consistent with results of prior studies, this strategy yielded dose-dependent responses, with those mice receiving larger doses of pulsed dendritic cells experiencing better therapeutic outcomes (ie, slower tumor growth).

For SPIO labeling of the harvested dendritic cells, we used protamine sulfate as a transfection agent, adapting a protocol previously implemented for labeling primary cells (23,39). This approach required a relatively short 3-hour period for labeling prior to footpad infection, thus differing somewhat from prior successful dendritic cell labeling studies requiring a 20-hour period for labeling with a FeREX agent or a 12-hour labeling period to image

dendritic cells with prostaglandin E2–enhanced migration. The protamine sulfate transfection protocol used for our study resulted in 100% labeling efficiency in only 3 hours and, importantly, demonstrated no significant differences in viability indexes between labeled and unlabeled dendritic cells. The short labeling period for this protocol may be more conducive to clinical translation during dendritic cell vaccination trials. Particularly given the potential fragility of harvested dendritic cells, a limited-duration labeling period could potentially avoid cell damage and subsequent alterations of priming function.

The SPIO labeling approach we used permitted MR imaging visualization of autologous dendritic cell migration from the left footpad into the draining LN. Dendritic cell accumulation was visualized as a reduction in T2-weighted signal intensity within the left popliteal LN at 6- and 24-hour intervals after footpad injection. No signal intensity alterations were observed within the right popliteal LN; this finding was consistent with histologic measurements, wherein no labeled dendritic cells were observed in the right popliteal LN. However, tumor growth was significantly suppressed for Panc02 tumors within both right and left flanks. Growth inhibition for both right and left flank tumors was well correlated with the T2-weighted SNR changes measured within the left popliteal LN 24 hours after injection. Each of the latter findings is suggestive of an enhanced systemic immune response initiated with footpad inoculation using these SPIO-labeled tumor antigen–pulsed autologous dendritic cells.

Our study had several limitations. First, MR imaging of SPIO-labeled dendritic cell migration was performed at only two time points after injection (6 and 24 hours), and our study protocol examined only two dendritic cell doses (1 and 2 million cells). Additional studies may be valuable to determine the optimal doses and optimal post-injection time intervals for follow-up imaging measurements. Furthermore, while our study utilized T2-weighted imaging measurements, quantitative voxelwise measurements should also be explored as an option to potentially enhance the reproducibility these measurements between patients in clinical settings. Finally, for these studies, the antitumor activity of the injected dendritic cells was assessed longitudinally with tumor size measurements. Prior studies using the Panc02 model with similar dendritic cell priming and vaccination approaches have already demonstrated that these methods induce tumor antigen–specific cytotoxic T-lymphocytes and inhibit growth. Future studies are clearly warranted to further study the impact of SPIO labeling on dendritic cell function.

Practical applications: In summary, our study demonstrated an efficient approach for *(a)* labeling primed dendritic cells within a 3-hour period and *(b)* noninvasive MR imaging visualization of migration to draining LNs. Signal intensity measurements on T2-weighted images significantly decreased following dendritic cell migration; these MR imaging measurements were well correlated with the longitudinal suppression of tumor growth in a murine pancreatic carcinoma model. These techniques may offer future insights into the dynamics and kinetics of dendritic cell migration in vivo and the related impact on therapeutic outcomes in both preclinical and clinical research settings. Additional translational studies are warranted to evaluate the efficacy of these approaches for early prediction of longitudinal outcomes during dendritic cell therapy in a broad range of tumor etiologies.

Disclosures of Conflicts of Interest: Z.Z. disclosed no relevant relationships. **W.L.** disclosed no relevant relationships. **D.P.** disclosed no relevant relationships. **K.L.** disclosed no relevant relationships. **A.Y.S.** disclosed no relevant relationships. **A.C.G.** disclosed no relevant relationships. **Y.G.** disclosed no relevant relationships. **K.K.** disclosed no relevant relationships. **Y.H.** disclosed no relevant relationships. **G.H.** disclosed no relevant relationships. **A.C.L.** disclosed no relevant relationships.

References

1. Lion E, Smits EL, Berneman ZN, Van Tendeloo VF. NK cells: key to success of DC-based cancer vaccines? Oncologist 2012;17(10):1256–1270.
2. Mocellin S, Mandruzzato S, Bronte V, Lise M, Nitti D. Part I: vaccines for solid tumours. Lancet Oncol 2004;5(11):681–689.
3. Karthaus N, Torensma R, Tel J. Deciphering the message broadcast by tumor-infiltrating dendritic cells. Am J Pathol 2012;181(3):733–742.
4. Hoos A, Eggermont AM, Janetzki S, et al. Improved endpoints for cancer immunotherapy trials. J Natl Cancer Inst 2010;102(18):1388–1397.
5. Aarntzen EH, De Vries IJ, Lesterhuis WJ, et al. Targeting CD4(+) T-helper cells improves the induction of antitumor responses in dendritic cell-based vaccination. Cancer Res 2013;73(1):19–29.
6. Tada F, Abe M, Hirooka M, et al. Phase I/II study of immunotherapy using tumor antigen-pulsed dendritic cells in patients with hepatocellular carcinoma. Int J Oncol 2012;41(5):1601–1609.
7. Palucka K, Banchereau J. Cancer immunotherapy via dendritic cells. Nat Rev Cancer 2012;12(4):265–277.
8. Pham W, Kobukai S, Hotta C, Gore JC. Dendritic cells: therapy and imaging. Expert Opin Biol Ther 2009;9(5):539–564.
9. Petersen TR, Dickgreber N, Hermans IF. Tumor antigen presentation by dendritic cells. Crit Rev Immunol 2010;30(4):345–386.
10. Zahradova L, Mollova K, Ocadlikova D, et al. Efficacy and safety of Id-protein-loaded dendritic cell vaccine in patients with multiple myeloma: phase II study results. Neoplasma 2012;59(4):440–449.
11. Oshita C, Takikawa M, Kume A, et al. Dendritic cell-based vaccination in metastatic melanoma patients: phase II clinical trial. Oncol Rep 2012;28(4):1131–1138.
12. Garcia-Marquez MA, Wennhold K, Draube A, von Bergwelt-Baildon M. Results of a phase II clinical trial with Id-protein-loaded dendritic cell vaccine in multiple myeloma: encouraging or discouraging? Immunotherapy 2012;4(10):991–994.
13. Martelli C, Borelli M, Ottobrini L, et al. In vivo imaging of lymph node migration of MNP- and (111)In-labeled dendritic cells in a transgenic mouse model of breast cancer (MMTV-Ras). Mol Imaging Biol 2012;14(2):183–196.
14. Srinivas M, Aarntzen EH, Bulte JW, et al. Imaging of cellular therapies. Adv Drug Deliv Rev 2010;62(11):1080–1093.
15. Ottobrini L, Martelli C, Trabattoni DL, Clerici M, Lucignani G. In vivo imaging of immune cell trafficking in cancer. Eur J Nucl Med Mol Imaging 2011;38(5):949–968.

16. de Vries IJ, Lesterhuis WJ, Barentsz JO, et al. Magnetic resonance tracking of dendritic cells in melanoma patients for monitoring of cellular therapy. Nat Biotechnol 2005;23(11):1407–1413.

17. Fleige G, Seeberger F, Laux D, et al. In vitro characterization of two different ultrasmall iron oxide particles for magnetic resonance cell tracking. Invest Radiol 2002;37(9):482–488.

18. Dekaban GA, Snir J, Shrum B, et al. Semiquantitation of mouse dendritic cell migration in vivo using cellular MRI. J Immunother 2009;32(3):240–251.

19. Baumjohann D, Hess A, Budinsky L, Brune K, Schuler G, Lutz MB. In vivo magnetic resonance imaging of dendritic cell migration into the draining lymph nodes of mice. Eur J Immunol 2006;36(9):2544–2555.

20. Muccioli M, Pate M, Omosebi O, Benencia F. Generation and labeling of murine bone marrow-derived dendritic cells with Qdot nanocrystals for tracking studies. J Vis Exp 2011 Jun 2;(52).

21. Nair SK, Snyder D, Rouse BT, Gilboa E. Regression of tumors in mice vaccinated with professional antigen-presenting cells pulsed with tumor extracts. Int J Cancer 1997;70(6):706–715.

22. Gigi V, Stein J, Askenasy N, Yaniv I, Ash S. Early immunisation with dendritic cells after allogeneic bone marrow transplantation elicits graft vs tumour reactivity. Br J Cancer 2013;108(5):1092–1099.

23. Zhang Z, Hancock B, Leen S, et al. Compatibility of superparamagnetic iron oxide nanoparticle labeling for ^{1}H MRI cell tracking with ^{31}P MRS for bioenergetic measurements. NMR Biomed 2010;23(10):1166–1172.

24. Zhang Z, Procissi D, Li W, et al. High resolution MRI for non-invasive mouse lymph node mapping. J Immunol Methods 2013;400-401(13):23–29.

25. Richert LE, Rynda-Apple A, Harmsen AL, et al. $CD11c^{+}$ cells primed with unrelated antigens facilitate an accelerated immune response to influenza virus in mice. Eur J Immunol 2014;44(2):397–408.

26. Susnik N, Sörensen-Zender I, Rong S, et al. Ablation of proximal tubular suppressor of cytokine signaling 3 enhances tubular cell cycling and modifies macrophage phenotype during acute kidney injury. Kidney Int 2014;85(6):1357–1368.

27. Bauer C, Bauernfeind F, Sterzik A, et al. Dendritic cell-based vaccination combined with gemcitabine increases survival in a murine pancreatic carcinoma model. Gut 2007;56(9):1275–1282.

28. Tanimoto A, Yuasa Y, Shinmoto H, et al. Superparamagnetic iron oxide-mediated hepatic signal intensity change in patients with and without cirrhosis: pulse sequence effects and Kupffer cell function. Radiology 2002;222(3):661–666.

29. Lutz MB, Schnare M, Menges M, et al. Differential functions of IL-4 receptor types I and II for dendritic cell maturation and IL-12 production and their dependency on GM-CSF. J Immunol 2002;169(7):3574–3580.

30. Grolleau-Julius A, Abernathy L, Harning E, Yung RL. Mechanisms of murine dendritic cell antitumor dysfunction in aging. Cancer Immunol Immunother 2009;58(12):1935–1939.

31. Ashley DM, Faiola B, Nair S, Hale LP, Bigner DD, Gilboa E. Bone marrow-generated dendritic cells pulsed with tumor extracts or tumor RNA induce antitumor immunity against central nervous system tumors. J Exp Med 1997;186(7):1177–1182.

32. Zitvogel L, Mayordomo JI, Tjandrawan T, et al. Therapy of murine tumors with tumor peptide-pulsed dendritic cells: dependence on T cells, B7 costimulation, and T helper cell 1-associated cytokines. J Exp Med 1996;183(1):87–97.

33. Paglia P, Chiodoni C, Rodolfo M, Colombo MP. Murine dendritic cells loaded in vitro with soluble protein prime cytotoxic T lymphocytes against tumor antigen in vivo. J Exp Med 1996;183(1):317–322.

34. Mayordomo JI, Loftus DJ, Sakamoto H, et al. Therapy of murine tumors with p53 wild-type and mutant sequence peptide-based vaccines. J Exp Med 1996;183(4):1357–1365.

35. Siders WM, Vergilis KL, Johnson C, Shields J, Kaplan JM. Induction of specific antitumor immunity in the mouse with the electrofusion product of tumor cells and dendritic cells. Mol Ther 2003;7(4):498–505.

36. Kim HS, Choo YS, Koo T, et al. Enhancement of antitumor immunity of dendritic cells pulsed with heat-treated tumor lysate in murine pancreatic cancer. Immunol Lett 2006;103(2):142–148.

37. Pan K, Zhao JJ, Wang H, et al. Comparative analysis of cytotoxic T lymphocyte response induced by dendritic cells loaded with hepatocellular carcinoma -derived RNA or cell lysate. Int J Biol Sci 2010;6(7):639–648.

38. Schnurr M, Scholz C, Rothenfusser S, et al. Apoptotic pancreatic tumor cells are superior to cell lysates in promoting cross-priming of cytotoxic T cells and activate NK and gammadelta T cells. Cancer Res 2002;62(8):2347–2352.

39. Zhang Z, van den Bos EJ, Wielopolski PA, et al. In vitro imaging of single living human umbilical vein endothelial cells with a clinical 3.0-T MRI scanner. MAGMA 2005;18(4):175–185.